

1 **Exploring the potential benefits of Ethanol Direct Injection (EDI) timing and**
2 **pressure on particulate emission characteristics in a Dual-Fuel Spark Ignition**
3 **(DFSI) engine**

4
5 **Xiang Li ^{a, b, *}, Dayou Li ^a, Jingyin Liu ^{c, *}, Tahmina Ajmal ^a, Abdel Aitouche ^{d, e}, Raouf Mobasher ^{d, e},**
6 **Oyuna Rybdylova ^f, Yiqiang Pei ^{b, *}, Zhijun Peng ^{g, *}**

7 ^a School of Computer Science and Technology, University of Bedfordshire, Luton, UK

8 ^b State Key Laboratory of Engines, Tianjin University, Tianjin, China

9 ^c School of Chemistry and Chemical Engineering, Nantong University, Nantong, China

10 ^d Univ. Lille, CNRS, Centrale Lille, UMR 9189 - CRISTAL - Centre de Recherche en Informatique Signal et
11 Automatique de Lille, F-59000 Lille, France

12 ^e Junia, Smart Systems and Energies, F-59000 Lille, France

13 ^f Advanced Engineering Centre, School of Architecture, Technology and Engineering, University of Brighton,
14 Brighton, UK

15 ^g School of Engineering, University of Lincoln, Lincoln, UK

16
17 *Corresponding author:

18 Xiang Li, School of Computer Science and Technology, University of Bedfordshire, Luton, LU1 3JU, UK

19 Email: xiang.li@beds.ac.uk

20 Jingyin Liu, School of Chemistry and Chemical Engineering, Nantong, China.

21 Email: jingyin.liu@ntu.edu.cn

22 Yiqiang Pei, State Key Laboratory of Engines, Tianjin University, Tianjin, China.

23 Email: peiyq@tju.edu.cn

24 Zhijun Peng, School of Engineering, University of Lincoln, Lincoln, LN6 7TS, UK

25 Email: jpeng@lincoln.ac.uk

26

27 **Abstract**

28 Nowadays, particulate matter emitted by vehicles severely impacts environmental quality and human
29 health. In this paper, the potential benefits of Ethanol Direct Injection (EDI) timing and pressure on
30 particulate emission characteristics in a Dual-Fuel Spark Ignition (DFSI) engine were initially and
31 systematically explored. The experimental results illustrate that by delaying EDI timing from -340
32 °CA to -300 °CA, there is a significant benefit in both particulate number and mass concentration.
33 Furthermore, the size distribution curve of particulate number changes from bimodal to unimodal,
34 meantime size distribution curves of particulate mass consistently concentrate on the accumulation
35 mode. By increasing EDI pressure from 5.5 MPa to 18 MPa, the droplet size of ethanol spray can be
36 effectively reduced. The benefit of increasing EDI pressure is more apparent in reducing particulate
37 number is than particulate mass. The concentration of number and mass for total particulates have a
38 reduction of 51.15% and 22.64%, respectively. In summary, it was demonstrated that an appropriate
39 EDI timing or high EDI pressure could be a practical and efficient way to reduce particulate emissions
40 in a DFSI engine.

41

42 **Keywords**

43 Dual-Fuel Spark Ignition (DFSI) engine; Particulate emissions; Ethanol; Injection timing; Injection
44 pressure

45

46 **1. Introduction**

47 Over the last decade, the impact of environmental pollution has been a global problem. One of
48 the major pollutants is particulate matter emitted by vehicles, which would adversely affect regional
49 air quality, climate change and human health, particularly cardiorespiratory diseases [1]. Currently,
50 some novel vehicle powertrain technologies without Internal Combustion Engine (ICE) have been
51 developed to reduce engine emissions, such as Battery Electric Vehicle (BEV) [2], Fuel Cell Electric
52 Vehicle (FCEV) [3][4], Oxy-Fuel Combustion-Carbon Capture and Storage (OFC-CCS) system [5].
53 However, the popularisation rate of these technologies is normally subject to cost, cruising range,
54 charging time and relevant supporting facilities [6][7]. Hence, particulate emissions from the ICE of
55 ICE-only vehicle, Hybrid Electric Vehicle (HEV) and Plug-in Hybrid Electric Vehicle (PHEV) have
56 attracted increasing attention from scholars in various fields [8][9].

57 With the advantages of superior volumetric efficiency, thermal efficiency, power output, and
58 transient response, Gasoline Direct Injection (GDI) engine has become an increasingly prevalent
59 option for ICE and vehicle manufacturers [10][11]. However, compared to Port Fuel Injection (PFI)
60 engine, particulate emissions of GDI engine are usually higher owing to higher spray impingement
61 possibility and shorter air-fuel mixing time [12]. Moreover, the regulations for particulate emissions
62 of GDI-powered vehicles have become more stringent in recent years. For example, in 2014 and 2017,
63 Euro 6b and Euro 6c standards limit the particulate number of GDI-powered vehicles to $6 \times 10^{12}/\text{km}$
64 and $6 \times 10^{11}/\text{km}$, respectively.

65 In order to reduce particulate emissions and keep the engine power performance, Dual-Fuel Spark
66 Ignition (DFSI) engine has been developed with the advantages of multiple fuel injection modes and
67 fuel properties [13]. Due to higher heating value and lower vaporisation latent heat, gasoline can be
68 used to contribute a better transient response, especially during engine cold start. As renewable fuels

69 with low carbon and high oxygen content, alcohol fuel can be utilised to reduce engine particulate
70 emissions and improve anti-knock performance by the advantage of higher octane.

71 The important research findings relevant to Dual-Fuel Spark Ignition (DFSI) engines are
72 summarised in Table 1. Daniel et al. [14] found that with the advantages of fuel injection flexibility,
73 Dual-Fuel Spark Ignition (DFSI) is very beneficial to optimise engine gaseous and particulate
74 emissions with changes in engine operating conditions. Kim et al. [15] demonstrated that both
75 reduction of particulate emissions and knock frequency could be achieved when ethanol port injection
76 is added. Liu et al. [16][17] compared different alcohol–gasoline and gasoline–alcohol injection
77 modes from a DFSI combustion engine. It was found that for selected engine operating conditions,
78 there is an optimal mass fraction for alcohol injection to optimise particulate matter emissions and
79 simultaneously keep fuel economy and power output. Catapano et al. [18] observed particulate
80 formation and emissions in an optical small DFSI engine fuelled with Compressed Natural Gas (CNG)
81 and gasoline. It was demonstrated that there is a benefit in reducing particulate emissions owing to
82 the gaseous properties of CNG. Kang et al. [19] systematically compared the effects of different
83 injection modes on combustion and knock suppression characteristics. Yu et al. [20][21] conducted
84 experimental studies about combustion and emissions in an SI engine, with ethanol/gasoline and
85 hydrous ethanol/gasoline dual-fuel injection modes. The studies concluded that the synergistic effects
86 of utilising ethanol injection and Exhaust Gas Recirculation (EGR) could effectively reduce gas and
87 particulate emissions. Furthermore, particulate size can be reduced by increasing the water ratio in
88 hydrous ethanol. Zhuang et al. [22][23] investigated the effects of different ethanol Direct Injection
89 (DI) timings on air-fuel mixture formation, combustion process, knock mitigation, Nitrogen Oxide
90 (NO) and Hydrocarbon (HC) emissions from a DFSI engine. It was indicated that ethanol DI timing
91 strongly influences the air-fuel mixture process and quality. Moreover, with the advance of ethanol

92 DI timing, the emissions are generally decreased.

93

94

Table 1. Important research findings concerning DFSI engines

Publication Year	Key Advances	Fuel	Main Authors
2013	Particulate emissions were investigated for ethanol injection under both dual-fuel injection and DI strategies.	Ethanol; Gasoline	Daniel et al. [14]
2014	Effects of ethanol injection timing on knock mitigation, lean-burn, NO and HC emissions were investigated from an SI engine with PFI-gasoline and DI-ethanol.	Ethanol; Gasoline	Zhuang et al. [22]
2015	Particulate emissions were investigated in an SI engine with PFI-ethanol and DI-gasoline with varying engine compression ratios and ethanol injection timings.	Ethanol; Gasoline	Kim et al. [15]
2015	The alcohol–gasoline and gasoline–alcohol DFSI combustion was compared for particulate reduction and fuel economy with varying alcohol mass fractions.	Methanol; Ethanol; Gasoline	Liu et al. [16][17]
2017	Particulate emissions were investigated in an optical small DFSI engine with DI-CNG and PFI-gasoline.	CNG; Gasoline	Catapano et al. [18]
2019	Effects of fuel injection modes on knock suppression were compared and studied under different injection modes on a single-cylinder SI engine.	Ethanol; Gasoline	Kang et al. [19]
2020	Effects of ethanol injection strategies on air-fuel mixture formation and combustion process were investigated from an SI engine with PFI-gasoline and DI-ethanol.	Ethanol; Gasoline	Zhuang et al. [23]
2021	The combustion and emissions were investigated with varying excess air ratios, ethanol direct injection ratios and exhaust recirculation ratios from an SI engine with PFI-gasoline and DI-ethanol.	Ethanol; Gasoline	Yu et al. [20]
2021	Effects of different water ratios in hydrous ethanol on combustion and emissions were investigated from an SI engine with PFI-gasoline and DI-hydrous ethanol.	Ethanol; Gasoline	Yu et al. [21]

95

96 As mentioned above, previous studies on the DFSI engine have proposed and investigated some
97 effective solutions to reduce engine emissions. However, regarding the fuel injection strategies of
98 DFSI engines, research findings mainly focused on the influence of fuel injection ratios and timings
99 on gaseous emissions. Besides, the effects of ethanol injection ratio on particulate emissions are
100 another existing hot topic. However, almost no systematic study on the effects of Ethanol Direct
101 Injection (EDI) timing and pressure on particulate emissions in a DFSI engine was reported.

102 Hence, the study presented in this paper concentrates on exploring the benefits of EDI timing and
103 pressure on particulate emission characteristics from a DFSI engine. The findings of this study would
104 help not only fill the gap of exploring EDI strategy on the reduction of particulate, but also provides
105 a fresh and practical way towards controlling the particulate problem of different kinds of vehicles.

106 **2. Experimental methodology**

107 *2.1. Experimental testbed and procedure*

108 The experimental study was performed on a dual-injection DFSI engine with the specifications
109 shown in Table 2. It is an advanced four-cylinder turbocharged engine with a displacement of 2.0-
110 litre and a compression ratio of 9.6. The fuel properties of gasoline and ethanol used in this study are
111 both presented in Table 3 [24]. Furthermore, as shown in Fig. 1, gasoline and ethanol are injected via
112 PFI injectors and DI injectors, respectively.

113

114

Table 2. Engine specifications

Items	Content
Engine type	4-cylinder, 4-stroke
Bore × Stroke (mm)	82.5 × 92
Displacement (L)	2.0
Injection mode	Dual-injection
Intake mode	Turbocharged
Compression ratio	9.6:1
Rated speed (rpm)	5500
Rated power (kW)	160
Maximum Torque (N·m)	320

115

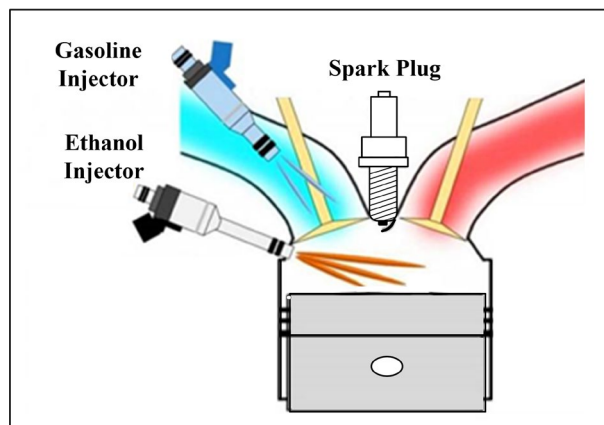
116

Table 3. Fuel properties [24]

Fuel type	Ethanol	Gasoline
Chemical formula	C ₂ H ₅ OH	C ₅ -C ₁₂
Relative molecular mass	46	95-120
Gravimetric oxygen content (%)	34.78	< 1
Research octane number	107	95

Density (20 °C) (kg/L)	0.789	0.73
Dynamic viscosity (20 °C) (mPa·s)	1.2	0.52
Kinematic viscosity (20 °C) (mm ² /s)	1.52	0.71
Surface tension (20 °C) (N/m)	21.97	22
Boiling range (°C)	78	30-200
Low heating value (kJ/kg)	26900	44300
Latent heat of vaporisation (kJ/kg)	840	370
Laminar flame speed (20 °C) (m/s)	0.5	0.33
Stoichiometric air-fuel ratio	8.95	14.7

117



118

119

Fig. 1. Schematic view of GPI plus EDI dual-injection system

120

121

Fig. 2 shows the schematic view of engine testbed. By using a programmable Electronic Control

122

Unit (ECU) and calibration software (INCA), an electrical dynamometer can measure and control

123

engine speed, torque and power output in real-time. Combustion characteristics can be calculated by

124

the transient signals of in-cylinder pressure, which were recorded and analysed via a combustion

125

measurement platform, including four high-precision spark-plug pressure sensors (AVL-GH13Z), an

126

encoder (Kistler-2614CK1), charge amplifiers (Kistler-5018A) and a combustion analyser (AVL-641).

127

In addition, the emission of particulates ranging from 5 nm to 1000 nm was measured by a fast

128

particulate analyser (Cambustion-DMS 500) connected to a sampling point in front of the engine's

129

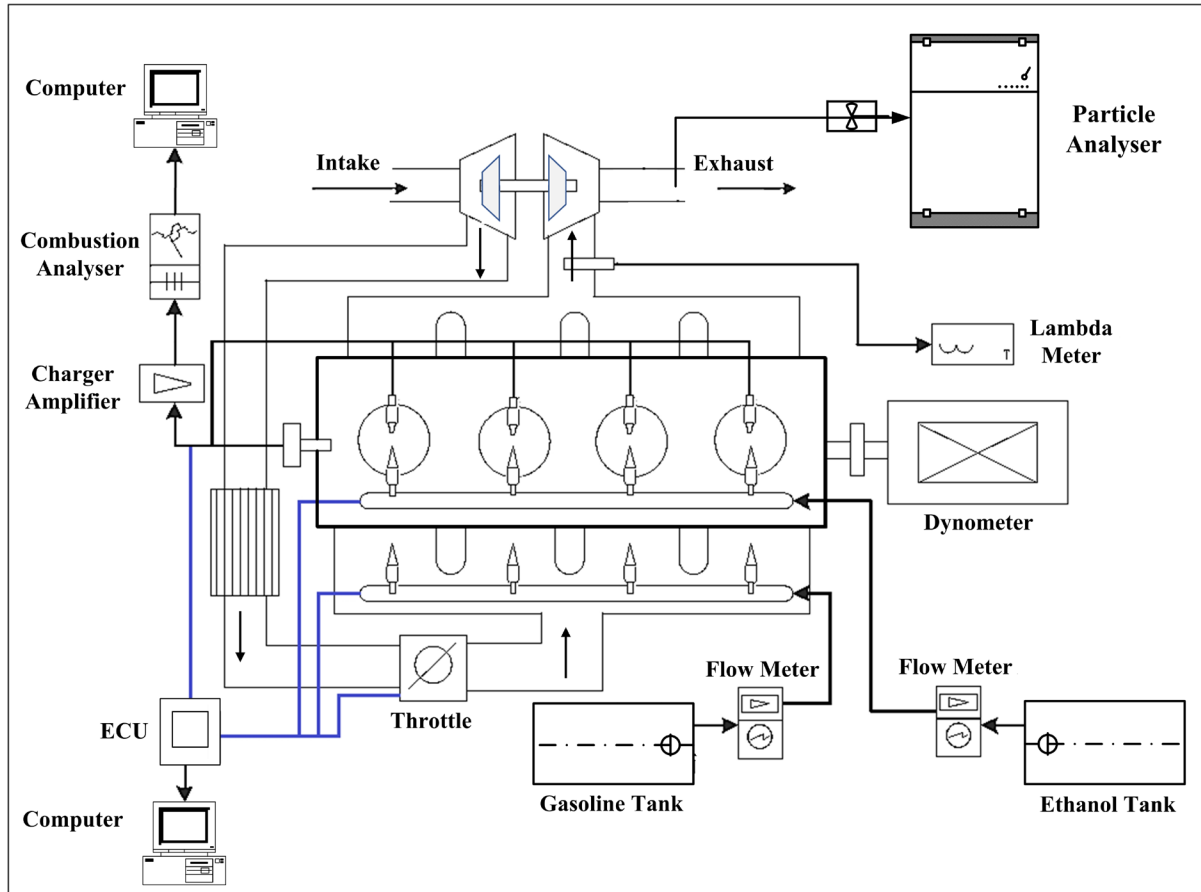
three-way catalytic converter. In this study, the engine operated at the speed of 2000 revolutions per

130

minute (rpm) and a typical low load of 2 bar Brake Mean Effective Pressure (BMEP). In order to

131 make the research process more efficient, the fuel injection mass ratio of PFI to DI was fixed at 1:1,
132 representing 50% gasoline-PFI plus 50% ethanol-DI.

133



134

135

136

137 In order to assure the accuracy of experimental results, Maximum Brake Torque (MBT) spark
138 timings were applied to all the engine operating conditions. The lambda, intercooler outlet
139 temperature and coolant were maintained at 1 ± 0.01 , 298 ± 2 K and 360 ± 2 K, respectively. The
140 combustion characteristics and particulate emissions data for each engine operating condition should
141 be recorded after the engine stabilises for two minutes. Furthermore, to minimise the impacts of cycle-
142 to-cycle variations, cylinder pressure result was averaged based on two hundred consecutive engine
143 cycles. Meanwhile, the result of particulate emissions was obtained from the average of repeated

144 measurements three times. Table 4 presents the uncertainties of some key parameters calculated by
145 Holman's root mean square method [25].

146

147 **Table 4.** Uncertainties of measured parameters

Measured Parameters	Uncertainty (%)
Engine speed	± 0.1
BMEP	± 0.1
BSFC	± 0.2
Pressure	± 0.1
Crank angle	± 0.1
Lambda	± 0.3
Coolant temperature	± 0.4
Intercooler output temperature	± 0.4
Particulate number	± 1.7

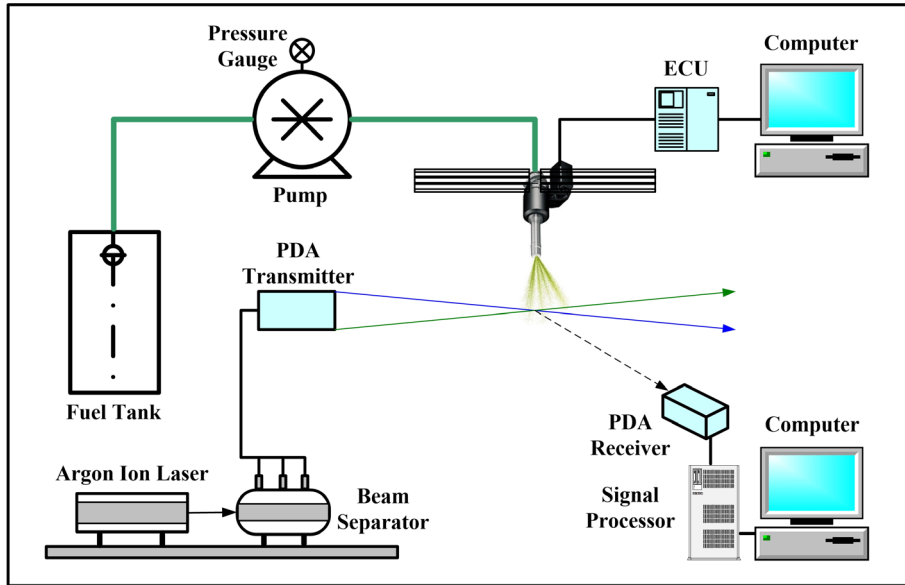
148

149 In order to make this research more comprehensive, the effects of EDI pressure on the droplet
150 diameter of ethanol spray from the engine's DI injector were studied via microscopic spray
151 characteristics investigation. Fig. 3 shows the Phase Doppler Particles Analyser (PDPA) system for
152 this investigation. With the advantage of an argon-ion laser, a 180 MHz high-frequency signal
153 processor and some other accessories, the PDPA system can provide accurate measurement results of
154 droplet diameter with a high resolution of 0.1 μm and a range from 0 to 236 μm . In order to match
155 with engine experiments, EDI pressure was set to be 5.5 MPa, 10 MPa, 14 MPa and 18 MPa in this
156 test. Furthermore, ethanol was injected into an ambient condition, which is 293 ± 0.5 K and 0.1 MPa.
157 An air extractor was utilised to help ensure the safety of experimental site.

158 Besides, as shown in Fig. 4, according to the Society of Automotive Engineers (SAE) J2715
159 standard [26], measurement points are selected at 50 mm downstream from the axial direction of the
160 nozzle. For minimising the interference of suspended fuel droplets of the latest injection, the ethanol
161 injection pulse and injection width were set to 0.1 Hz and 1.2 ms, respectively. To ensure

162 measurement accuracy, 20000 validated sample droplets were collected for each experimental
163 condition, and the collection should be repeated three times.

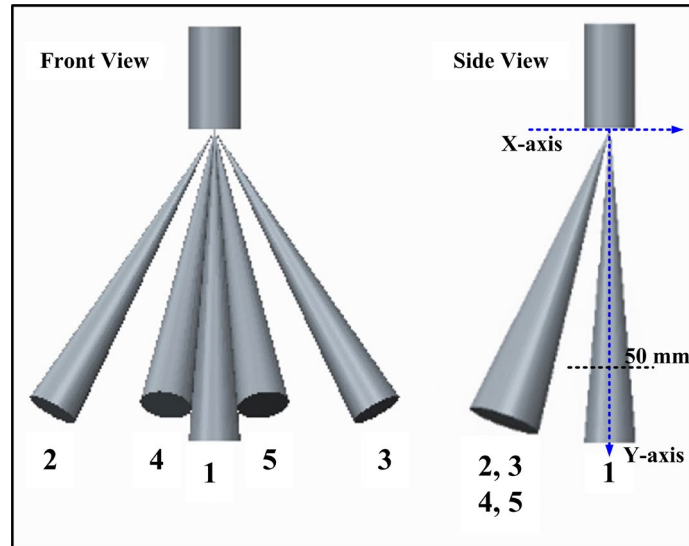
164



165

166

Fig. 3. Schematic view of PDPA system



167

168

Fig. 4. Measurement points of PDPA test

169 2.2. Key parameters in this study

170 In this study, some key parameters are introduced and defined to help better under the
171 characteristics of combustion and particulate emissions. t_I and P_I denote EDI timing and EDI
172 pressure, respectively. θ_F denotes ignition delay, representing Crank Angle (CA) interval between

173 spark timing and φ_{CA10} (where 10% of cumulative heat has released). θ_C denotes combustion
 174 duration, representing CA interval between φ_{CA10} and φ_{CA90} (where 90% of cumulative heat has
 175 released). φ_{CA50} denotes the CA where 50% of cumulative heat has released. R_M and T_M denote
 176 maximum heat release rate and maximum in-cylinder temperature, respectively. η_B denotes engine
 177 brake thermal efficiency, as shown in Equation (1).

$$178 \quad \eta_B = \frac{p_B}{M_G \times H_G + M_E \times H_E} \times 100\% \quad (1)$$

179 Here, p_B is engine brake power. M_G and M_E are the mass flow rate of gasoline and ethanol,
 180 respectively. M_G and M_E are the mass flow rate of gasoline and ethanol, respectively. H_G and H_E
 181 are the low heating value of gasoline and ethanol, respectively.

182 Regarding the parameters of particulate emissions, D_p , N_p and M_p denote particulate diameter,
 183 particulate number and particulate mass, respectively. For each particulate, the calculation of
 184 converting D_p to M_p is shown in Equation (2) [27][28].

$$185 \quad M_p(\mu\text{g}) = 1.72 \times 10^{-15} \times D_p^{2.65}(\text{nm}) \quad (2)$$

186 Besides, in the PDPA test, D_d denotes diameter of droplet; D_{SMD} denotes Sauter mean diameter
 187 of droplets; D_{sub} denotes the difference of D_{SMD} between $P_I = 5$ MPa and other P_I (10 MPa, 14
 188 MPa and 18 MPa) conditions.

189 3. Results and discussion

190 3.1. Optimising engine particulate emission characteristics by changing EDI timing

191 In the section, the characteristics of particulate emission are investigated by changing t_I from -
 192 340 °CA to -280 °CA. Meantime, P_I is fixed at base value, which is 5.5 MPa.

193 Fig. 5 shows the effects of t_I on θ_F , θ_C , φ_{CA50} and η_B . On the whole, combustion phasing
 194 characterised by θ_F , θ_C and φ_{CA50} is not significantly affected by t_I , but some key features can
 195 also be observed.

196 With the delay of t_I from -340 °CA to -280 °CA, θ_F slightly increases from 27.06 degrees to
197 27.37 degrees, meantime θ_C has a reduction of 0.68 degrees. Besides, the variation of φ_{CA50} is
198 generally stable with the delay of t_I . As a result, η_B shows a slight improvement of 0.21 percent.
199 This can be attributed to a combined effect of three factors. First, as the earliest injection condition
200 ($t_I = -340$ °CA) is very near to Top Dead Centre (TDC), it is easy to cause fuel impingement on the
201 piston crown, slowing down the rate of fuel vaporisation. Hence, delaying t_I to -280 °CA would help
202 reduce the possibility of fuel impingement, which is beneficial to promote air-fuel mixture. Second,
203 under $t_I = -280$ °CA, θ_C becomes shorter which helps reduce the heat transfer to combustion
204 chamber walls. Third, by delaying t_I , the homogeneity of air-fuel mixture would be reduced owing
205 to a shorter mixing time. It would lead to a negative impact on η_B , but it cannot offset the first two
206 benefits.

207 Fig. 6 and Fig. 7 show the effects of t_I on cylinder pressure and heat release rate, respectively.
208 It is demonstrated that there is no obvious change in the curves of cylinder pressure and heat release
209 rate by changing t_I . The main feature is that with the delay of t_I from -340 °CA to -280 °CA, there
210 is a slight rise in the peak of the curve. Fig. 8 presents the effects of t_I on R_M and T_M . It can be
211 seen that with the delay of t_I , R_M shows a general gradual increase of 0.56 J/CA. In the meantime,
212 T_M is a bit lower when t_I is -320 °CA and -300 °CA, but it keeps around 2575 K on the whole,
213 which indicates that the probability of particulate oxidation is not greatly affected by the variation of
214 T_M under different conditions of t_I .

215

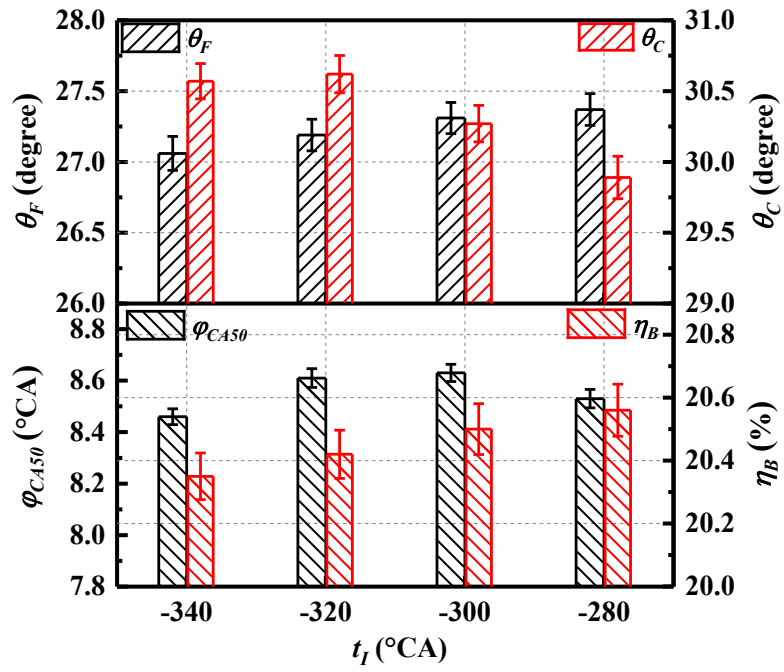


Fig. 5. Effects of t_l on θ_F , θ_C , φ_{CA50} and η_B

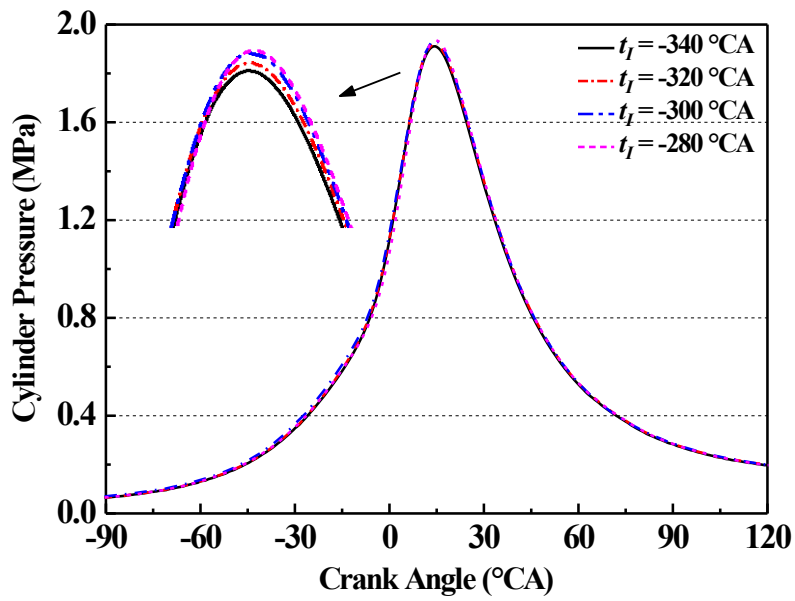


Fig. 6. Effects of t_l on cylinder pressure

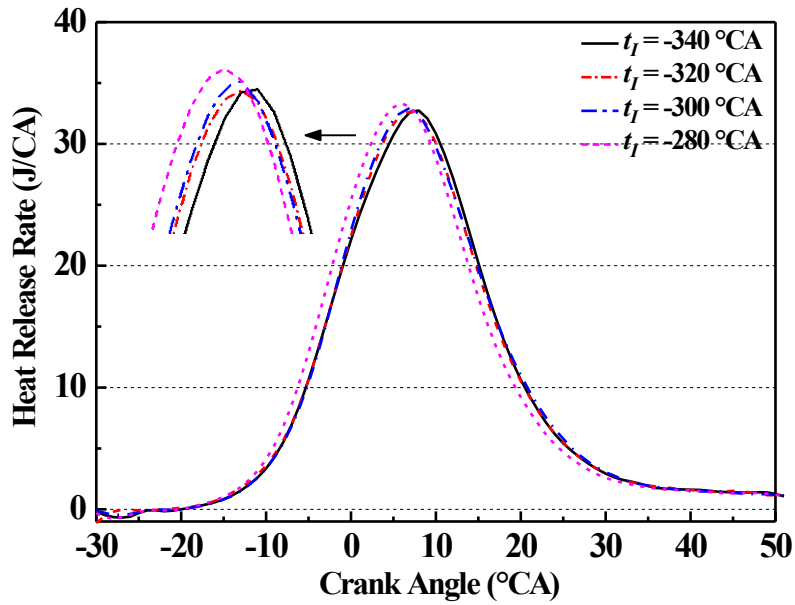


Fig. 7. Effects of t_l on heat release rate

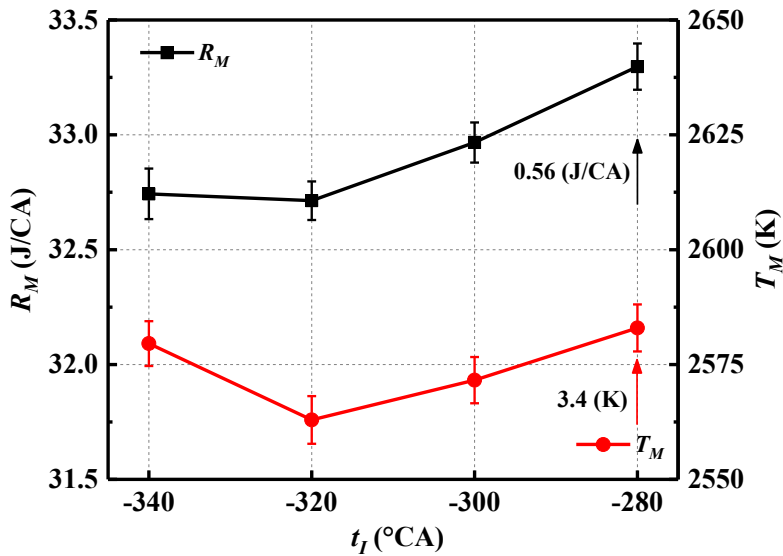


Fig. 8. Effects of t_l on R_M and T_M

220

221

222

223

224

225

226

227

228

229

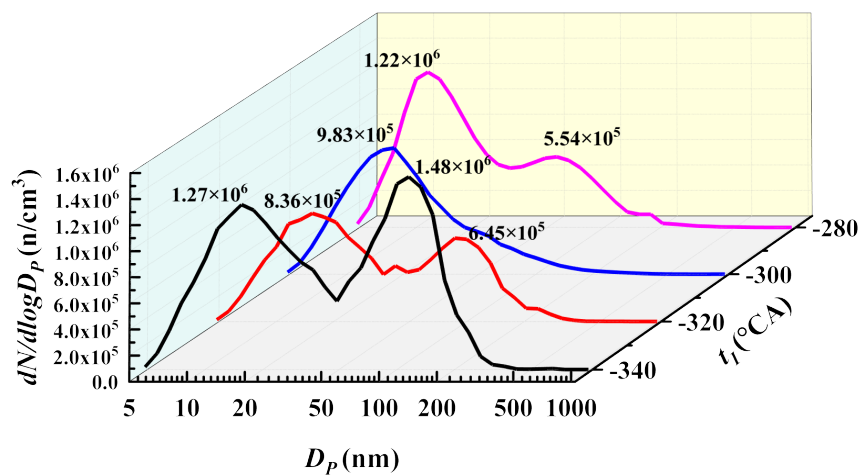
230

Fig. 9 shows the effects of t_l on N_p size distribution. It can be seen that the N_p size distribution is quite sensitive to t_l . With t_l from -340 °CA to -320 °CA, the peak of curve for nucleation mode decreases from 1.27×10^6 to 8.36×10^5 , whilst the peak of accumulation mode decreases from 1.48×10^6 to 6.45×10^5 . By delaying t_l to -300 °CA, the curve changes from bimodal to unimodal. However, it would increase again and change to be bimodal again with the further delay of t_l to -280 °CA. This is mainly because when t_l is -340 °CA, the piston has just passed through

231 the TDC. The spray impingement possibilities will be significantly increased, as the fuel injector is
 232 relatively close to piston crown. When t_I is -280°CA , heterogeneous mixture will also be enhanced
 233 by less time between t_I and spark timing compared to that of $t_I = -300^\circ\text{CA}$. Besides, Hydrogen-
 234 Abstraction-Acetylene-Addition (HACA) growth rates would be increased with a higher T_M when
 235 t_I is -340°CA and -280°CA [29][30]. Thus, the quality of air-fuel mixture has deteriorated, leading
 236 to higher emissions of N_p .

237 Fig. 10 shows the effects of t_I on M_p size distribution. Regardless of t_I , M_p size distribution
 238 almost concentrates on the accumulation mode, meantime M_p of nucleation mode is very low.
 239 Besides, the highest M_p curve can be seen under the condition of $t_I = -340^\circ\text{CA}$ due to the largest
 240 N_p of accumulation mode under this condition.

241



242

243

Fig. 9. Effects of t_I on N_p size distribution

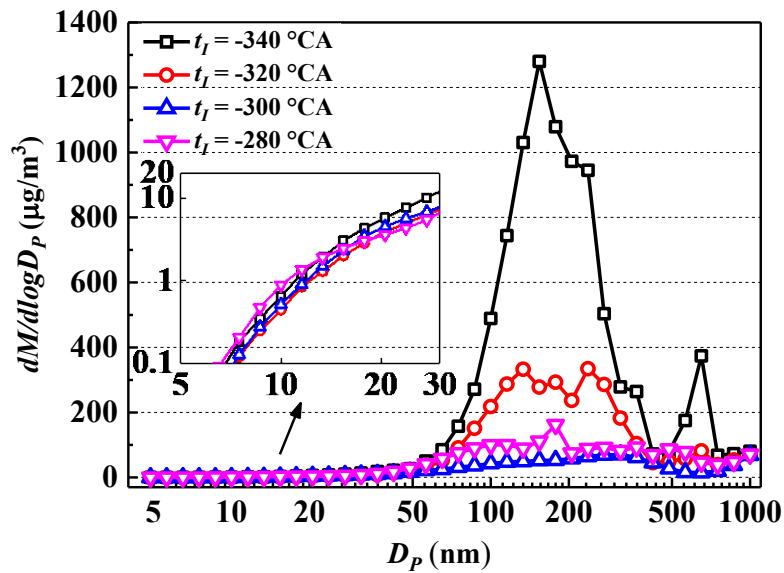


Fig. 10. Effects of t_I on M_P size distribution

244

245

246

247 In order to better understand the effects of t_I on particulate emissions at a macroscopic level,

248 Fig. 11 and Fig. 12 presents the N_P and M_P concentrations with varying t_I , respectively.

249 It can be seen that both N_P and M_P concentrations are very sensitive to changing t_I . On the

250 whole, an appropriate t_I is very helpful to decrease particulate emissions. By delaying t_I from -

251 340 °CA to -300 °CA, there is a significant reduction of 54.65 % and 89.15% in N_P concentration

252 and M_P concentration of total particulates, respectively. But the immediate cause of reduction for

253 N_P concentration is not very similar to that of M_P . Under $t_I = -300$ °CA, although N_P of

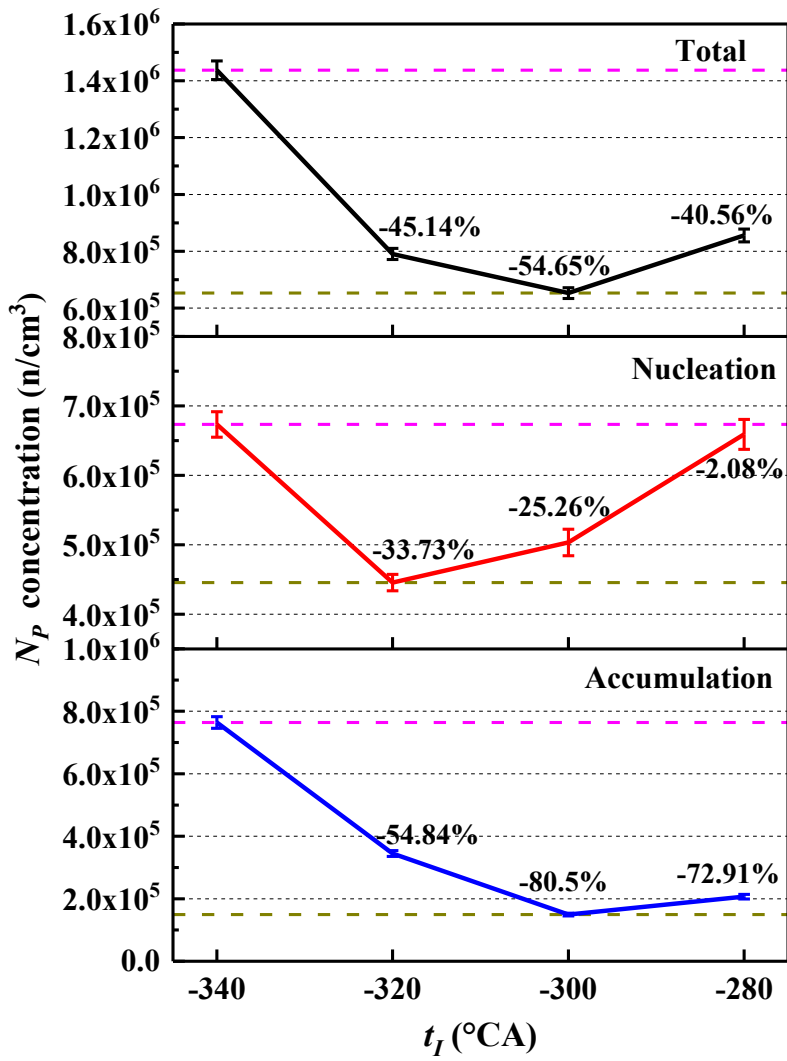
254 nucleation mode is a bit higher than that of $t_I = -320$ °CA owing to the less air-fuel mixture time,

255 N_P concentration of total particulates is still lower under $t_I = -300$ °CA by the significant reduction

256 in accumulation particulates. Regarding the M_P concentration, M_P of nucleation mode can be

257 neglected, so M_P concentration of total particulates is closely related to accumulation mode.

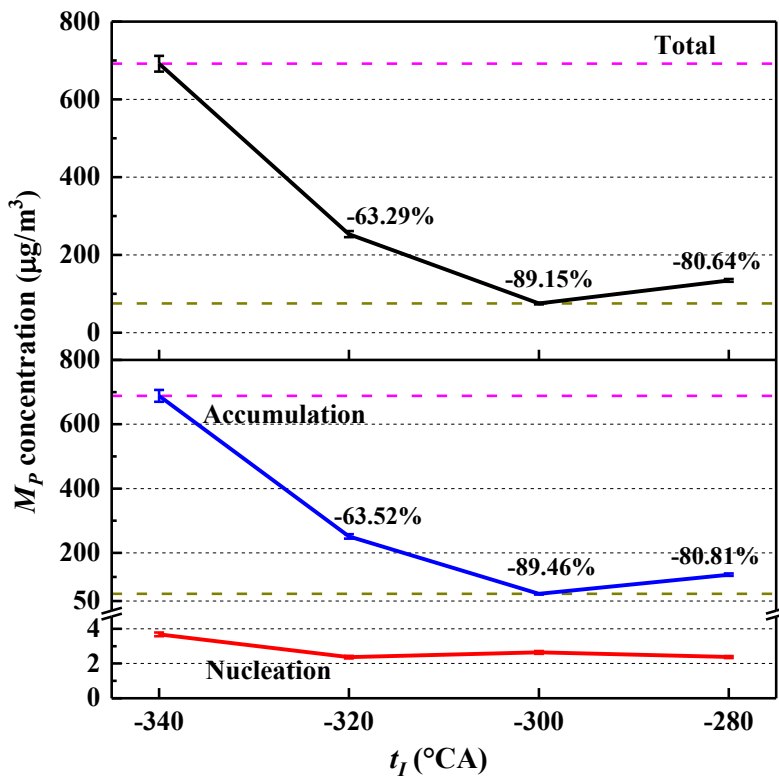
258



259

260

Fig. 11. Effects of t_I on N_p concentration for nucleation, accumulation and total particulates



261

262

Fig. 12. Effects of t_I on M_p concentration for nucleation, accumulation and total particulates

263

3.2. Optimising engine particulate emission characteristics by EDI pressure

264

This section mainly focuses on the experimental results by changing P_I from 5.5 MPa to 18 MPa,

265

which covers the P_I common range of most commercial GDI and DFSI engines. Moreover, t_I is

266

fixed at -300 °CA in the meantime.

267

Fig. 13 presents the effects of P_I on p_d of D_d at (0, 50). It can be seen that with the increase

268

of P_I from 5.5 MPa to 18 MPa, a steady decline can be found in the p_d of large droplets which D_d

269

is more than 20 μm . Furthermore, the concentration of D_d moves to smaller size droplets. The

270

position and p_d of curve's peak respectively change to 6 μm and 14.8% under $P_I = 18$ MPa, while

271

the corresponding values are respectively 10 μm and 11.55% under $P_I = 5.5$ MPa.

272

Regarding the whole view of droplet size at 50 mm of jet downstream, Fig. 14 shows the effects

273

of P_I on both D_{SMD} and D_{Sub} for different locations. It was found that increasing P_I can

274

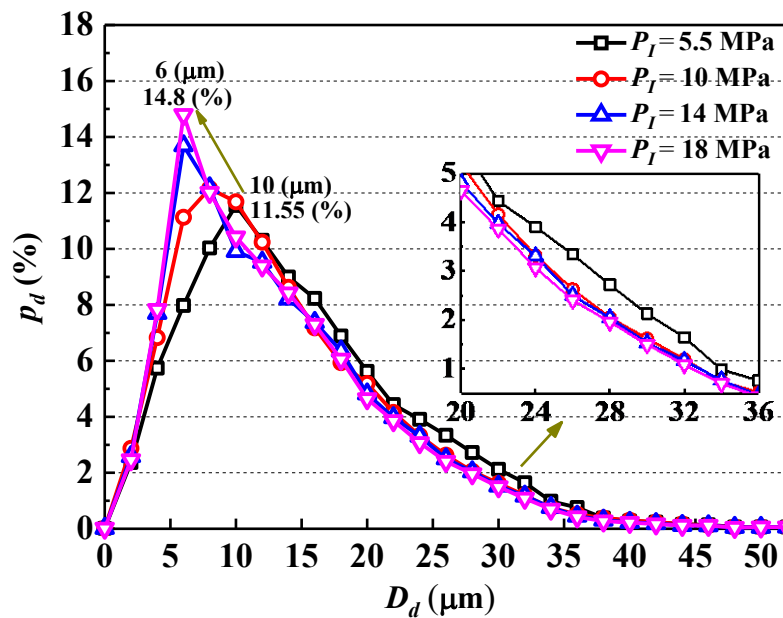
effectively decrease D_{SMD} regardless of the locations, which would promote the progress of

275

secondary atomisation, evaporation and air-fuel mixing. Besides, the comparison of D_{Sub} of

276 different P_I denotes that a reduction of around $1.7 \mu\text{m}$ can be observed for every 4 MPa increase of
 277 P_I . Another interesting observation is that D_{SMD} of $(-12, 50)$ and $(12, 50)$ is larger than locations.
 278 This explanation can be that the bulk of the spray breaks into filaments and droplets during the
 279 primary atomisation, increasing the collision probability between droplets inside the spray boundary.
 280 In the meantime, the breakup rate is increased by the shearing force outside the spray boundary,
 281 reducing the D_{SMD} of $(-16, 50)$ and $(16, 50)$. As a result, the curves present a general distribution of
 282 bimodal under all conditions of P_I .

283



284

285

Fig. 13. Effects of P_I on p_d of D_d at $(0, 50)$

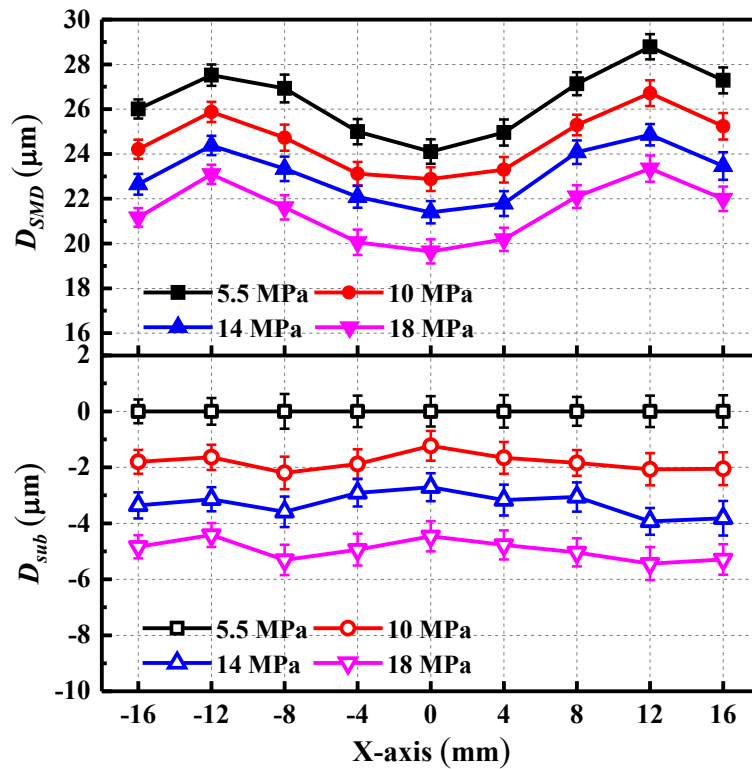


Fig. 14. Effects of P_I on D_{SMD} and D_{Sub} at 50 mm of jet downstream

286

287

288

289

290

291

292

293

294

295

296

297

298

299

300

Fig. 15 presents the effects of P_I on θ_F , θ_C , φ_{CA50} and η_B . It can be seen that increasing P_I could reduce the combustion duration, even though the effect is not apparent. With the increase of P_I from 5.5 MPa to 18 MPa, θ_F and θ_C each reduces 0.72 degrees and 0.47 degrees, meanwhile φ_{CA50} slightly advances from 8.63 °CA to 8.51 °CA. This is because the air-fuel mixture quality is improved with the reduction of D_{SMD} owing to higher P_I . A shorter combustion duration would mitigate the waste heat between high-temperature gases and in-cylinder wall, leading to a benefit of 0.13 percent in η_B . Fig. 16 and Fig. 17 present the variations of cylinder pressure and heat release rate with varying P_I . On the whole, both of them are not significantly affected by P_I . The main characteristic is that a slight advance and improvement can be observed for the curve' peak by increasing P_I . Fig. 18 further shows that there is a gradual increase of R_M and T_M with the increase of P_I , which could help promote fuel burn rate, leading to a benefit in η_B .

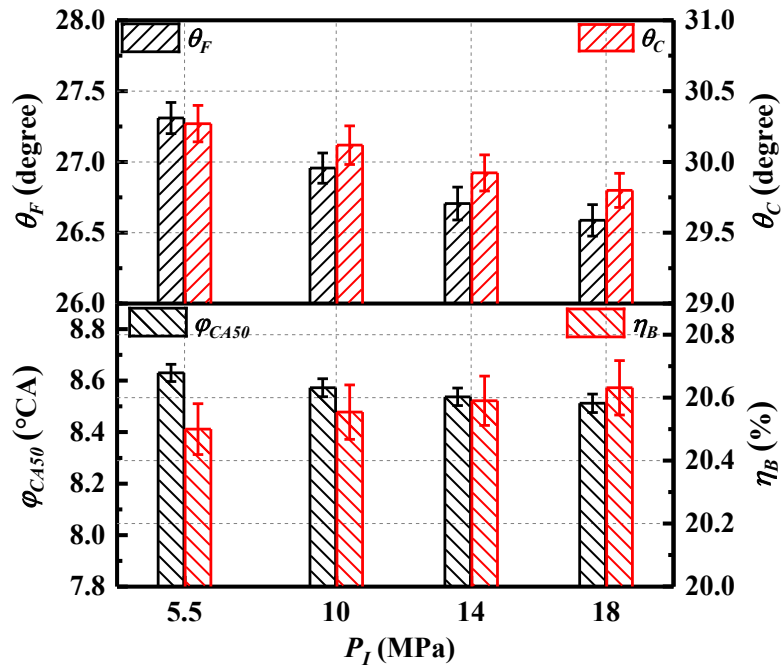


Fig. 15. Effects of P_I on θ_F , θ_C , φ_{CA50} and η_B

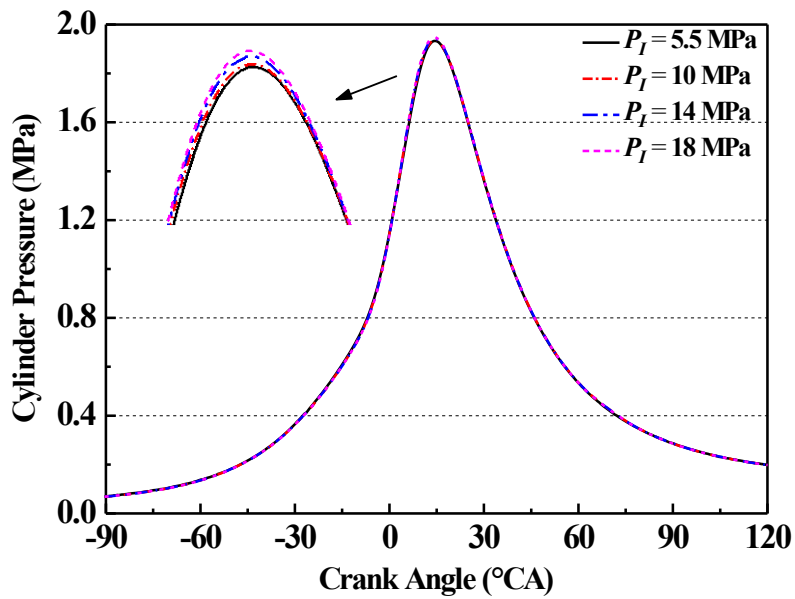


Fig. 16. Effects of P_I on cylinder pressure

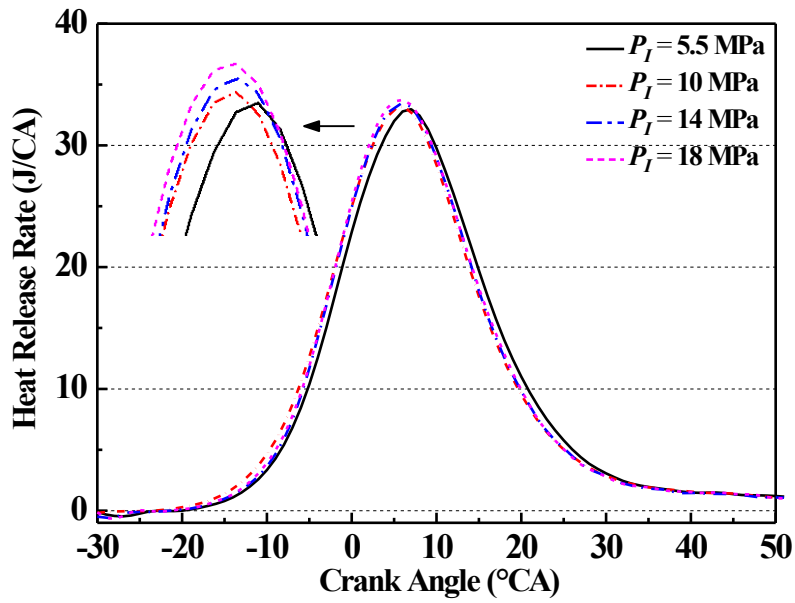


Fig. 17. Effects of P_I on heat release rate

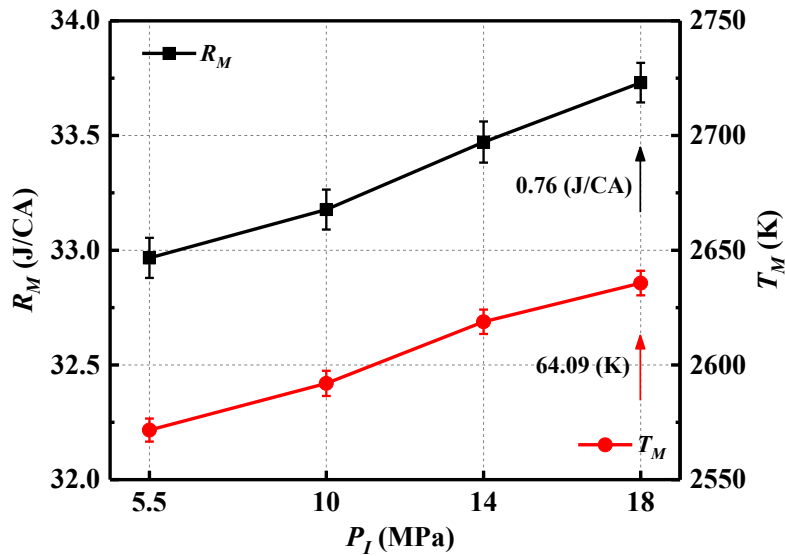


Fig. 18. Effects of P_I on R_M and T_M

305

306

307

308

309

310

311

312

313

314

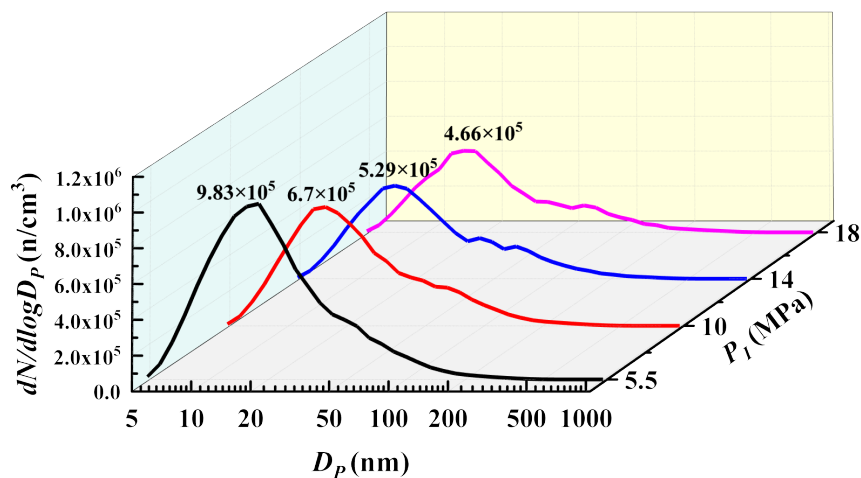
315

Fig. 19 and Fig. 20 show the effects of P_I on size distribution of N_p and M_p , respectively. It can be observed that every N_p curve presents an approximate unimodal distribution with a peak located around 17 nm nucleation mode. Furthermore, by increasing P_I from 5.5 MPa to 18 MPa, the peak of N_p curve gradually reduces from 9.83×10^5 to 4.66×10^5 . Regarding the trend of M_p , it demonstrates that increasing P_I has a positive effect on M_p reduction, but the benefit is not very obvious. The curve shape of M_p size distribution remains stable, and the curve peak concentrates

316 around 300 nm D_p . Besides, because a large nucleation particulate is much heavier than nucleation
 317 particulates, an increment can be seen for D_p more than 600 nm in the M_p curves. But due to the
 318 very small N_p , the absolute value of M_p is still very low, which is less than 70 at 1000 nm.

319 Fig. 21 and Fig. 22 can visually explain the effects of P_I on N_p and M_p in a macroscopic view.
 320 With the increase of P_I from 5.5 MPa to 18 MPa, the concentration of N_p and M_p for total
 321 particulates decrease by 51.15% and 22.64%, respectively. The reduction of M_p is far less than that
 322 of N_p . Moreover, M_p concentration of total particulates is closely related to that of accumulation
 323 mode, which presents a gradual decline trend with increased P_I . This is because regardless of P_I ,
 324 EDI mode would have the appearance of spray impingement, which causes the heterogeneous mixture
 325 around piston crown region. Although higher P_I is helpful to air-fuel mixture quality, the
 326 heterogeneous mixture by spray impingement and pool fires cannot be entirely avoided, which is a
 327 dominant source of accumulation mode particulates. Besides, Fig. 18 has demonstrated that higher
 328 in-cylinder temperature can be seen with increased P_I , which would further gain the advantage of
 329 promoting particulate oxidation by ethanol as an oxygenated fuel, providing a benefit in the reduction
 330 of N_p and M_p .

331



332

333

Fig. 19. Effects of P_I on N_p size distribution

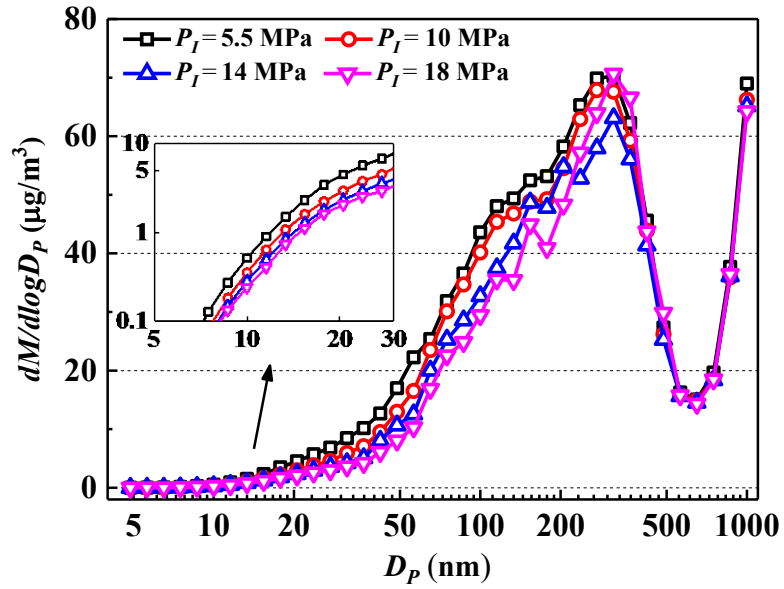


Fig. 20. Effects of P_I on M_P size distribution

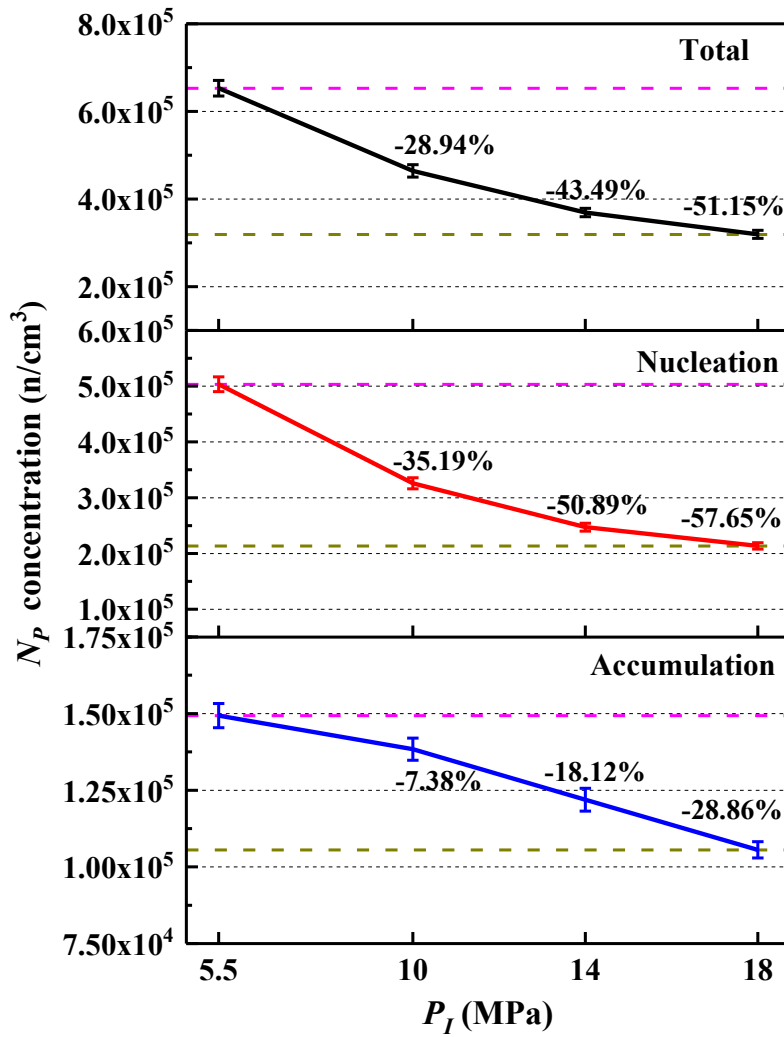
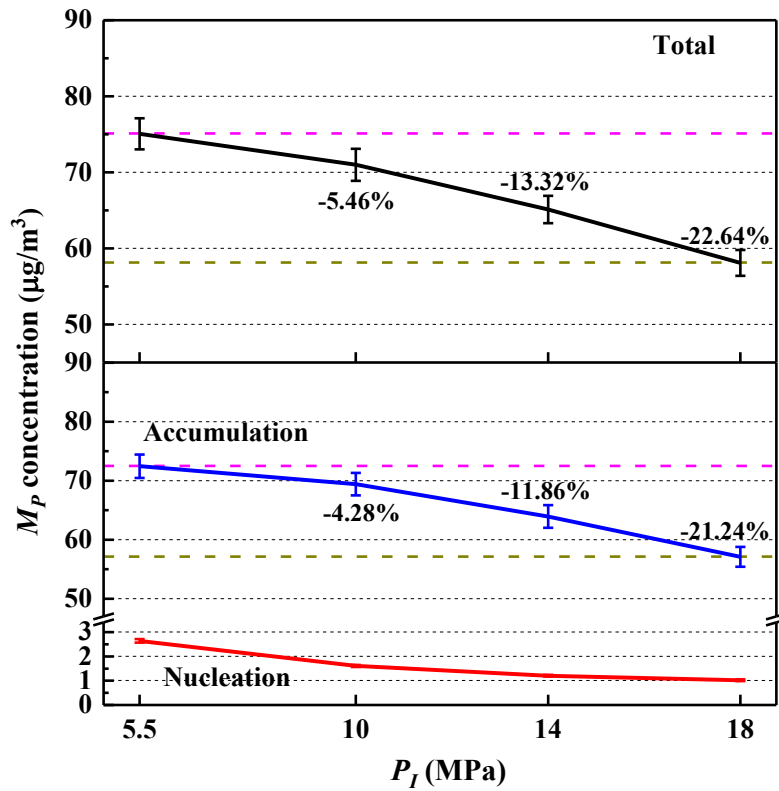


Fig. 21. Effects of P_I on N_P concentration for nucleation, accumulation and total particulates



338

339

Fig. 22. Effects of P_I on M_P concentration for nucleation, accumulation and total particulates

340

4. Conclusions

341

342

343

344

345

346

347

348

349

350

351

In order to develop more environmentally friendly vehicles, particulate emissions from ICE have been a serious problem to solve. The importance of this study is that the potential benefits of EDI timing and pressure on particulate emissions are systematically explored in a DFSI engine under PFI-gasoline and DI-ethanol mode. The findings can offer some original and fresh insights into the implementation of ethanol combined with the injection strategy of controlling particulate emissions regarding the DFSI engine. The main results of this study can be drawn as follows.

- (1) With the delay of t_I from -340 °CA to -280 °CA, θ_C has a reduction of 0.68 degrees. The variations of θ_F and φ_{CA50} are generally stable. In the meantime, a slight improvement of 0.21 percent in η_B can be achieved.
- (2) It is a highly effective way to optimise engine particulate emission characteristics by changing t_I . By delaying t_I from -340 °CA to -300 °CA, there is a significant reduction of 54.65 %

352 and 89.15% in N_p concentration and M_p concentration of total particulates, respectively.
353 Furthermore, the curve of N_p size distribution changes from bimodal to unimodal. Under
354 all conditions, M_p size distribution almost concentrates on the accumulation mode.

355 (3) Increasing P_I would promote the progress of secondary atomisation, evaporation and air-
356 fuel mixing for the ethanol spray. By increasing P_I from 5.5 MPa to 18 MPa, the position
357 and p_d of curve's peak respectively change to 6 μm and 14.8% from 10 μm and 11.55%.
358 D_{SMD} can be effectively reduced.

359 (4) By increasing P_I from 5.5 MPa to 18 MPa, the gradual increase of R_M and T_M could help
360 promote fuel burn rate. θ_F and θ_C each reduce 0.72 degrees and 0.47 degrees, meanwhile
361 φ_{CA50} slightly advances from 8.63 °CA to 8.51 °CA, leading to a benefit of 0.13 percent in
362 η_B .

363 (5) Regardless of P_I , N_p curve presents an approximate unimodal distribution with a peak
364 located around 17 nm nucleation mode. With the increase of P_I to 18 MPa, it is more
365 apparent in the reduction of N_p is than that of M_p . The concentration of N_p and M_p for
366 total particulates decrease by 51.15% and 22.64%, respectively.

367

368 **CRedit authorship contribution statement**

369 **Xiang Li:** Conceptualization, Methodology, Formal analysis, Investigation, Data curation,
370 Visualization, Writing - original draft. **Dayou Li:** Formal analysis. **Jingyin Liu:** Writing - reviewing
371 & editing. **Tahmina Ajmal:** Project administration. **Abdel Aitouche:** Project administration, Funding
372 acquisition. **Raouf Mobasher:** Project administration. **Oyuna Rybdylova:** Writing - reviewing &
373 editing. **Yiqiang Pei:** Methodology, Project administration, Funding acquisition. **Zhijun Peng:**
374 Methodology, Writing - reviewing & editing.

375 **Declaration of Competing Interest**

376 The authors declare that they have no known competing financial interests or personal
377 relationships that could have appeared to influence the work reported in this paper.

378

379 **Acknowledgement**

380 This work is financially supported by the National Engineering Laboratory for Mobile Source
381 Emission Control Technology (No. NELMS2017C01), and the European Regional Development
382 Fund (ERDF) via Interreg North-West Europe (Project No. NWE553).

383

384 **Reference**

- 385 [1] Awad, O.I., Ma, X., Kamil, M., Ali, O.M., Zhang, Z., Shuai, S., 2020. Particulate emissions from gasoline direct
386 injection engines: A review of how current emission regulations are being met by automobile manufacturers.
387 *Sci. Total Environ.* 718, 137302.
- 388 [2] Lyu, Y., Siddique, A.R.M., Majid, S.H., Biglarbegian, M., Gadsden, S.A., Mahmud, S., 2019. Electric vehicle
389 battery thermal management system with thermoelectric cooling. *Energy Rep.* 5, 822-827.
- 390 [3] Song, Z., Pan, Y., Chen, H., Zhang, T., 2021. Effects of temperature on the performance of fuel cell hybrid
391 electric vehicles: A review. *Appl. Energy* 302, 117572.
- 392 [4] Usai, L., Hung, C.R., Vásquez, F., Windsheimer, M., Burheim, O.S., Strømman, A.H., 2021. Life cycle
393 assessment of fuel cell systems for light duty vehicles, current state-of-the-art and future impacts. *J.*
394 *Cleaner Prod.* 280, 125086.
- 395 [5] Li, X., Peng, Z., Pei, Y., Ajmal, T., Rana, K.J., Aitouche, A., Mobasher, R., 2022. Oxy - fuel combustion for
396 carbon capture and storage in internal combustion engines – A review. *Int. J. Energy Res.* 46(2), 505-522.
- 397 [6] Guo, J., Jiang, Y., Yu, Y., Liu, W., 2020. A novel energy consumption prediction model with combination of
398 road information and driving style of BEVs. *Sustainable Energy Technologies and Assessments*, 42, 100826.
- 399 [7] Li, L., Guo, S., Cai, H., Wang, J., Zhang, J., Ni, Y., 2020. Can China's BEV market sustain without government
400 subsidies?: An explanation using cues utilization theory. *J. Cleaner Prod.* 272, 122589.
- 401 [8] Qian, Y., Li, Z., Yu, L., Wang, X., Lu, X., 2019. Review of the state-of-the-art of particulate matter emissions
402 from modern gasoline fueled engines. *Appl. Energy* 238, 1269-1298.
- 403 [9] Ge, J.C., Wu, G., Choi, N.J., 2022. Comparative study of pilot–main injection timings and diesel/ethanol binary
404 blends on combustion, emission and microstructure of particles emitted from diesel engines. *Fuel*, 313, 122658.
- 405 [10] Chen, Z., Zhang, Y., Wei, X., Zhang, Q., Wu, Z. and Liu, J., 2017. Thermodynamic process and performance
406 of high n-butanol/gasoline blends fired in a GDI production engine running wide-open throttle (WOT). *Energy*
407 *Convers. Manage.* 152, 57-64.

- 408 [11] Han, D., Fan, Y., Sun, Z., Nour, M., Li, X., 2020. Combustion and emissions of isomeric butanol/gasoline
409 surrogates blends on an optical GDI engine. *Fuel* 272, 117690.
- 410 [12] Huang, Y., Surawski, N.C., Zhuang, Y., Zhou, J.L., Hong, G., 2021. Dual injection: An effective and efficient
411 technology to use renewable fuels in spark ignition engines. *Renewable Sustainable Energy Rev.* 143,
412 110921.
- 413 [13] Ikoma, T., Abe, S., Sonoda, Y., Suzuki, H., Suzuki, Y., Basaki, M., 2006. Development of V-6 3.5-liter engine
414 adopting new direct injection system (No. 2006-01-1259). SAE Technical Paper.
- 415 [14] Daniel, R., Xu, H., Wang, C., Richardson, D., Shuai, S., 2013. Gaseous and particulate matter emissions of
416 biofuel blends in dual-injection compared to direct-injection and port injection. *Appl. Energy* 105, pp.252-261.
- 417 [15] Kim, N., Cho, S., Min, K., 2015. A study on the combustion and emission characteristics of an SI engine under
418 full load conditions with ethanol port injection and gasoline direct injection. *Fuel* 158, 725-732.
- 419 [16] Liu, H., Wang, Z., Long, Y., Xiang, S., Wang, J., Fatouraie, M., 2015. Comparative study on alcohol–gasoline
420 and gasoline–alcohol Dual-Fuel Spark Ignition (DFSI) combustion for engine particle number (PN) reduction.
421 *Fuel* 159, 250-258.
- 422 [17] Liu, H., Wang, Z., Long, Y., Xiang, S., Wang, J., Wagon, S.W., 2015. Methanol-gasoline Dual-fuel Spark
423 Ignition (DFSI) combustion with dual-injection for engine particle number (PN) reduction and fuel economy
424 improvement. *Energy* 89, 1010-1017.
- 425 [18] Catapano, F., Di Iorio, S., Sementa, P., Vaglieco, B.M., 2017. Particle formation and emissions in an optical
426 small displacement SI engine dual fueled with CNG DI and gasoline PFI (No. 2017-24-0092). SAE Technical
427 Paper.
- 428 [19] Kang, R., Zhou, L., Hua, J., Feng, D., Wei, H., Chen, R., 2019. Experimental investigation on combustion
429 characteristics in dual-fuel dual-injection engine. *Energy Convers. Manage.* 181, 15-25.
- 430 [20] Zhao, Z., Yu, X., Huang, Y., Shi, W., Guo, Z., Li, Z., Du, Y., Jin, Z., Li, D., Wang, T., Li, Y., 2022.
431 Experimental study on combustion and emission of an SI engine with ethanol/gasoline combined injection and
432 EGR. *J. Cleaner Prod.* 331, 129903.
- 433 [21] Li, D., Yu, X., Du, Y., Xu, M., Li, Y., Shang, Z., Zhao, Z., 2022. Study on combustion and emissions of a
434 hydrous ethanol/gasoline dual fuel engine with combined injection. *Fuel* 309, 122004.
- 435 [22] Zhuang, Y., Hong, G., 2014. Effects of direct injection timing of ethanol fuel on engine knock and lean burn in
436 a port injection gasoline engine. *Fuel* 135, 27-37.
- 437 [23] Zhuang, Y., Ma, Y., Qian, Y., Teng, Q., Wang, C., 2020. Effects of ethanol injection strategies on mixture
438 formation and combustion process in an ethanol direct injection (EDI) plus gasoline port injection (GPI) spark-
439 ignition engine. *Fuel* 268, 117346.
- 440 [24] Li, X., Pei, Y., Ajmal, T., Rana, K.J., Aitouche, A., Mobasher, R., Peng, Z., 2021. Numerical investigation on
441 implementing Oxy-Fuel Combustion (OFC) in an ethanol-gasoline Dual-Fuel Spark Ignition (DFSI) engine.
442 *Fuel*, 302, 121162.
- 443 [25] Holman, J.P., 1966. *Experimental methods for engineers*. New York, NY: McGraw-Hill.
- 444 [26] Hung, D.L., Harrington, D.L., Gandhi, A.H., Markle, L.E., Parrish, S.E., Shakal, J.S., Sayar, H., Cummings,
445 S.D., Kramer, J.L., 2009. Gasoline fuel injector spray measurement and characterization—a new SAE J2715
446 recommended practice. *SAE International Journal of Fuels and Lubricants* 1(1), 534-548.

- 447 [27] Symonds, J.P.R., 2010. Calibration of fast response differential mobility spectrometers. National Physical Lab.,
448 Metrology of Airborne Nanoparticles, Standardisation and Applications, London.
- 449 [28] Chen, L., Liang, Z., Zhang, X., Shuai, S., 2017. Characterizing particulate matter emissions from GDI and PFI
450 vehicles under transient and cold start conditions. *Fuel* 189, 131-140.
- 451 [29] Wang, H., Frenklach, M., 1997. A detailed kinetic modeling study of aromatics formation in laminar premixed
452 acetylene and ethylene flames. *Combust. Flame* 110(1-2), 173-221.
- 453 [30] Sun, W., Hamadi, A., Abid, S., Chaumeix, N., Comandini, A., 2020. An experimental and kinetic modeling
454 study of phenylacetylene decomposition and the reactions with acetylene/ethylene under shock tube pyrolysis
455 conditions. *Combust. Flame* 220, 257-271.